Eur. Phys. J. D **11**, 207–212 (2000)

THE EUROPEAN PHYSICAL JOURNAL D

EDP Sciences

Predissociation resonances in CO and IBr. Smooth exterior scaling combined with the discrete variable representation

H.O. Karlsson[a]

Department of Quantum Chemistry, Uppsala University, Box 518, 751 20 Uppsala, Sweden

Received 12 July 1999 and Received in final form 6 December 1999

Abstract. Smooth exterior scaling (SES) and the discrete variable representation (DVR) are combined to accurately compute predissociation resonances of a bound state non-adiabatically coupled to a dissociative state. For the CO($B^1\Sigma^+ - D'^1\Sigma^+$) predissociation interaction good agreement is found with approaches based on optical potentials and complex scaling. The comparison is done both in the diabatic and the adiabatic representation. The effect of the coupling strength in the IBr ($B^3\Pi_{0+} - Y0^+$) predissociation interaction and the transition from the diabatic to the adiabatic picture was studied by computing resonances for coupling strengths from 50 cm^{-1} up to 300 cm^{-1}. The transition from weak (diabatic) to strong (adiabatic) coupling was clearly seen. The intermediate case leads to a complicated resonance distribution. Comparison was made with recent studies using pump-probe spectroscopy [M. Shapiro, M.J.J. Vrakking, A. Stolow, J. Chem. Phys. **110**, 2465 (1999)]. It was found that the overall features of the experiment could be explained from the resonance distribution, but for a detailed comparison more accurate potential energy surfaces and couplings are needed.

PACS. 33.80.Gj Diffuse spectra; predissociation, photodissociation – 02.70.Jn Collocation methods – 33.70.Jg Line and band widths, shapes, and shifts

1 Introduction

Potential energy surfaces (PES) is a central concept in chemical physics. It allows the description of chemical phenomena as taking place on a single PES picturing, *e.g.*, the motion of wave packets from reactants to products. With modern quantum chemical techniques accurate PES for up to, at least, four atom systems are available for computing reactive processes.

The PES are a consequence of the Born-Oppenheimer (B-O) approximation, the decoupling of the nuclear and electronic degrees of freedom, which is normally assumed valid, at least in the region close to the equilibrium. Recent experimental techniques have however made it possible to probe processes far from equilibrium and for an accurate description of these photochemical processes we must go beyond the B-O approximation and include non-adiabatic couplings between several PES [1]. Many processes are in fact driven by this coupling. One such example, which we will study here, is predissociation caused by a non-adiabatic coupling between a bound and a dissociative state, giving rise to predissociation resonances $E_{\rm res} = E - {\rm i}\Gamma/2$.

To compute the CO($B^1\Sigma^+ - D'^1\Sigma^+$) predissociation resonances Monnerville and Robbe [2,3] used a combination of the discrete variable representation (DVR) and optical (absorbing) potentials (OP). In the DVR the Hamiltonian is discretized on a grid and the potential will then be a diagonal matrix whereas the kinetic energy operator will be represented as a full matrix. Two of the most common choices of DVR are the Fourier Grid Hamiltonian (FGH) [4] and the sinc DVR [5,6]. The FGH is based on a Fourier basis and thus has periodic boundary conditions whereas the sinc-DVR is zero at the boundaries, being based on particle-in-a-box functions. Another way of viewing the DVR is as a infinite order finite difference scheme. The sinc-DVR can in fact be derived as a limiting case of finite differences [6]. An advantage of the DVR is that no integrals need to be performed. The PES, normally given as a set of data points, needs only to be interpolated at the grid points. For coupled systems, as studied here, the coupling will be a diagonal matrix whereas for a basis set approach it will be a full matrix.

The popularity of absorbing potentials stems mainly from the ease with which they are implemented in the DVR: an imaginary (or complex) potential is simply added to the Hamiltonian $H \rightarrow H + V_{\rm op}$ The extra potential has the property of being zero in the interaction region and "turning on" in the "un-physical" region where there are no interaction, *i.e.* the PES is constant. A number of different forms of $V_{\rm op}$ are used and work well for, *e.g.*, cross-sections where broad resonances dominate. Accurate computation of single resonances is more difficult but can be done as shown for CO in [2,3]. However, the use

[a] e-mail: hans.karlsson@kvac.uu.se

of absorbing potentials are very empirical and there are no mathematical proofs that it converges to the correct resonance values.

A method that does stand on a solid mathematical ground is complex scaling (CS). It is based on a similarity transformation of the Hamiltonian such that outgoing boundary conditions are imposed and the wave functions remains square integrable. It is normally implemented through the coordinate transformation $r \rightarrow re^{i\theta}$ (θ is a real scaling angle), defining a path in the complex plane. The theory has been successfully applied to a number of problems in atomic and molecular physics [7]. Bound states and resonances are independent of the scaling angle whereas continuum states will rotate with θ. For a finite basis, however, the resonances will only be locally independent of the scaling angle, *i.e.* they will have a small dependence on θ. Problems arise how to implement the coordinate transformation when the potential is not dilation analytic or is given as a set of grid points. One solution to the problem is to use a finite basis set representation (FBR) and scale the basis functions rather than the Hamiltonian. The problem is then transfered to evaluation of the integral of complex basis functions with a real potential. In the context of predissociation Li *et al.* [8] used complex scaled harmonic oscillator basis functions to compute the resonances in CO, with excellent results. However, for numerical potentials one still needs a grid to compute the integral on with, *e.g.* Gaussian quadrature [8].

A method that combines the best of the OP and CS methods is the smooth exterior scaling (SES) [7,9–11]. In the SES the coordinate is kept real until some distance x_0 after which it smoothly moves out in the complex plane. It has the same mathematical rigor as complex scaling (which it is based on) and the same feature as an optical potential that it "turns on" outside the interaction region. The difference with OP is mainly the way it is applied: the kinetic energy will be modified instead of adding an empirical extra potential.

The aim of this paper is to show that the DVR-SES approach can be used to accurately compute predissociation resonances and be implemented as easily as the DVR-OP approach. In Section 2 we will review the SES and in Section 3 we apply the DVR-SES approach to the $CO(B^1\Sigma^+ - D'^1\Sigma^+)$ predissociation interaction and compare with the DVR-OP and FBR-CS methods both in the diabatic and adiabatic representation. In Section 4 we compute the predissociation resonances of the IBr $(B^3\Pi_{0+} - Y0^+)$ interaction to see how the resonances change with increasing coupling strength. An comparison with recent experiments are also done. Section 5 summarizes the results.

2 Smooth exterior scaling

Smooth exterior scaling can be implemented *via* a coordinate transformation [7,9–11]

$$z = F(x), \qquad f(x) = \frac{\mathrm{d}}{\mathrm{d}x}F(x), \tag{2.1}$$

that defines a path in the complex plane, leading to a transformed Hamiltonian

$$H = -\frac{1}{2m}\frac{1}{f(x)}\frac{\mathrm{d}^2}{\mathrm{d}x^2}\frac{1}{f(x)} + V_k(x) + V(F(x)), \tag{2.2}$$

$$V_k(x) = \frac{1}{8m}\left(2f''(x)f(x) - 3[f'(x)]^2\right)/f^4(x). \tag{2.3}$$

From a DVR point of view this means that the kinetic energy matrix is unchanged. It needs only be pre- and post-multiplied with a diagonal matrix

$$\mathbf{H} = \mathbf{M}\ \mathbf{T}\ \mathbf{M} + \mathbf{V}_k + \mathbf{V} \tag{2.4}$$

where $\mathbf{M}_{ii} = 1/f(x_i)$ and $\mathbf{V}_k$ and $\mathbf{V}_k$ are diagonal matrices.

The complex path $F(x)$ is chosen according to the same philosophy as the OP: it stays on the real axis in the interaction region and then smoothly moves out in the complex plane. Here a Woods-Saxon form [10] has been used

$$f(x) = 1 + (e^{i\theta} - 1)[1 + e^{(x_0 - x)/\epsilon}]^{-1} \tag{2.5}$$

where x_0 is the "turn on" point and ϵ is the width of the "turn on" region.

An important point to notice is that if the PES is constant in the outer region it is not affected by the scaling (a constant is not scaled). In other words, for a numerically given potential which takes a constant value beyond x_0 only the kinetic energy operator is scaled. Note the similarity with the optical potentials.

3 Predissociation resonances in CO

The $CO(B^1\Sigma^+ - D'^1\Sigma^+)$ Rydberg valence predissociation interaction is chosen for a comparison between the different methods. Monnerville and Robbe used the DVR-OP approach in both the diabatic [2] and adiabatic [3] representations to compute the predissociation resonances, as did Li *et al.* [8] but using the FBR-CS approach.

The system, depicted in Figure 1, consists of a dissociative state crossing a bound state at $R_c = 1.307$ Å. The diabatic coupling element is constant inside the crossing and decays to zero at large inter-nuclear separation as a Gaussian function. Potentials and the coupling are given in reference [2] and the procedure by Parlant and Yarkony [12] was used to transform from the diabatic to the adiabatic picture.

The lowest 11 resonance states, both in the adiabatic and the diabatic representation were computed using the parameters from Monnerville and Robbe [2,3]. The number of grid points was 200 and the parameters for the Woods-Saxon complex path was $x_0 = 1.8$ and $\epsilon = 0.20$. The computations were done for several values of the scaling angle θ and a resonance was considered converge when it did not change with θ [8]. Theoretically the resonances are independent of the scaling angle but the finite representation induces a small θ dependence. The continuum

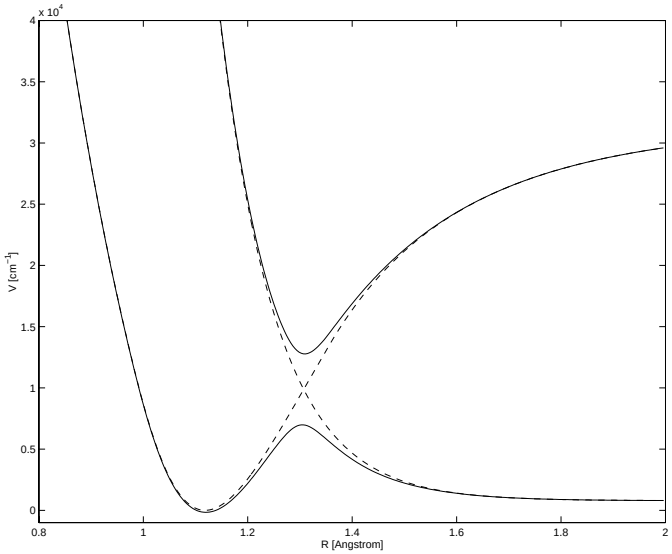

Fig. 1. The $B(^1\Sigma^+)$ and $(D'^1\Sigma^+)$ potential energy surfaces for CO in the adiabatic (solid line) and diabatic (dashed line) representation.

states will vary much more with θ and the resonances are easily identified. In computation of cross-sections only a single scaling angle is normally needed [13].

In Table 1 we compare our result for the diabatic and adiabatic representations with that of Monnerville and Robbe [2,3] and Li *et al.* [8]. The agreement between the different methods are good. The small discrepancies might be due to the RKR fit of the $B^1\Sigma^+$ state, the diabatic to adiabatic transformation or how to determine the convergence of a resonance state. The DVR-SES approach can thus be used with confidence for computing predissociation resonances.

4 Predissociation resonances in IBr

The interest in the predissociation interaction of the $B(^3\Pi_{0+})$ and $Y(0^+)$ states of IBr goes back to the experiments by Sedin [14] in the early 1960's. There are two competing channels

$$\mathrm{IBr} + h\nu \rightarrow \begin{cases} \mathrm{I}(^2\mathrm{P}_{3/2}) + \mathrm{Br}^*(^2\mathrm{P}_{1/2}) \\ \mathrm{I}(^2\mathrm{P}_{3/2}) + \mathrm{Br}(^2\mathrm{P}_{3/2}) \end{cases} \qquad (4.1)$$

with the last one correlating with the ground state. The spin-orbit coupling is of intermediate strength, as was discussed in the seminal paper by Child [15] from 1976, which means that the system cannot be explained from a pure diabatic or adiabatic picture. In a recent study by Vrakking *et al.* [16] and Shapiro *et al.* [17] ultrafast pump-probe spectroscopy was used to study the influence of the intermediate coupling strength on wave-packet dynamics. Ten different wave-lengths from the crossing region up to the $\mathrm{I}(^2\mathrm{P}_{3/2}) + \mathrm{Br}^*(^2\mathrm{P}_{1/2})$ dissociation threshold was used. They found that the pump-probe signal differed considerably for the different wave-lengths from

Table 1. The first 11 predissociation resonances for the $\mathrm{CO}(B^1\Sigma^+ - D'^1\Sigma^+)$ interaction, computed both in the adiabatic and diabatic representation. Absolute value of difference with the DVR-OP [3] and the FBR-CS [8] methods are also shown. Units is in cm^{-1}.

	Energy					
		Diabatic			Adiabatic	
ν	This work	Ref. [8]	Ref. [3]	This work	Ref. [8]	Ref. [3]
0	905.38	0.13	0.01	905.38	0.13	0.00
1	2988.67	9.76	0.38	2988.82	0.39	0.53
2	4971.15	0.54	0.38	4971.15	0.54	0.38
3	6783.80	0.29	0.12	6783.80	0.29	0.12
4	8514.57	0.10	0.10	8514.60	0.01	0.13
5	10 628.90	0.44	0.12	10 628.95	0.05	0.05
5	13 226.47	2.34	1.97	13 228.70	0.01	0.27
7	14 713.05	0.24	0.01	14 713.16	0.00	0.12
8	16 922.31	0.30	0.02	16 922.40	0.43	0.12
9	17 533.85	0.27	0.01	17 533.93	0.07	0.06
10	19 437.44	0.21	0.01	19 437.49	0.16	0.03
	Width					
		Diabatic			Adiabatic	
ν	This work	Ref. [8]	Ref. [3]	This work	Ref. [8]	Ref. [3]
0	0.00	0.000	0.000	0.000	0.000	0.000
1	0.0004	0.000	0.000	0.0004	0.000	0.000
2	0.8947	0.004	0.000	0.8877	0.007	0.150
3	90.86	0.040	0.030	91.04	0.140	0.140
4	801.3	0.500	0.500	801.3	0.500	0.000
5	1854	0.000	0.000	1854	0.000	0.000
6	2149	0.000	0.000	2150	1.000	1.000
7	9.387	0.009	0.002	9.366	0.032	0.020
8	1191	0.000	0.000	1191	0.000	0.000
9	622.3	0.400	0.100	622.3	0.400	0.300
10	0.2884	0.003	0.001	0.2897	0.004	0.002

a rapid decay close to the crossing region to more complex oscillations close to dissociation. A simulation of the pump-probe signal was done using the artificial channel method [18]. Although the main features were reproduced there was a shift in energy compared to the experimental findings. Hussain and Roberts [19] analyzed the same experiment using wave-packet propagation methods with similar findings. The nonadiabatic coupling strength used varied between 90 cm^{-1} [17] and 150 cm^{-1} [19].

The aim here is firstly to illustrate the transition from weak (diabatic) to strong (adiabatic) coupling and how the resonance distribution is affected. Secondly the resonances for $V_\mathrm{c} = 90$ cm^{-1} and $V_\mathrm{c} = 150$ cm^{-1} are computed for comparison with the work by Shapiro *et al.* [17] and Hussain and Roberts [19]. The system is modelled using the potentials from Guo [20] (see Fig. 2). The diabatic bound $B(^3\Pi_{0+})$ is a fit to a Morse potential and the dissociative $Y(0^+)$ is modelled as a decaying exponential. For a laser pulse of 90 fs, as used in the experiments

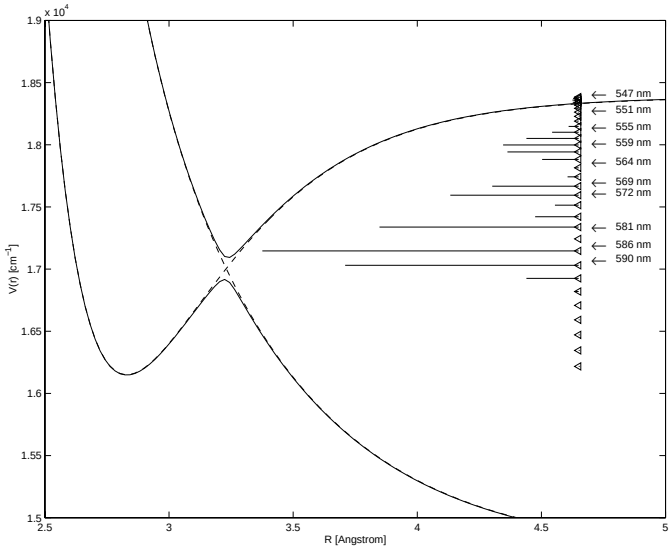

Fig. 2. The $B(^3\Pi_{0+})$ and $Y(0^+)$ potential energy surfaces for IBr in the adiabatic (solid line) and diabatic (dashed line) representation. The arrows indicate the excitation wave-lengths used by Shapiro *et al.* [17]. Triangles marks the position of the resonances and the lines are proportional to the width Γ and inversely proportional to the lifetime τ.

[17], about five to eight states contributes to the wave-packet. In Figure 3 the resonances for $V_c = 50$, 100, 150, 200, 250 and 300 cm^{-1} are depicted. We have also indicated with arrows the positions of avoided crossing maxima and minima for each coupling strength. The lowest states have long lifetimes but as the coupling strength increases they move out in the complex plane. Already for $V_c = 200$ cm^{-1} the formation of a dissociation threshold for the lower adiabat is clearly seen. In the upper region the resonances lies close to the real axis for $V_c = 50$ cm^{-1} being close to the diabatic bound states. As the coupling strength increases they move out in the complex plane but with further increase they move back to the real axis to form (nearly) bound states in the upper bound adiabatic surface. In the region of intermediate strength the distribution of resonances is non-trivial, clearly showing that neither the diabatic nor the adiabatic picture is valid.

There have been some discussion about the strength of the coupling and if it can be considered as constant or not. Shapiro *et al.* [17] used a constant coupling of strength $V_c = 90$ cm^{-1} whereas Hussain and Roberts [19] used $V_c = 150$ cm^{-1}. In Figure 4 the lifetimes $\tau = \hbar/\Gamma$ for the resonances for the two coupling strengths are shown. The lifetimes are also given in Table 2 together with the nearest-neighbour distances. (The numbering relates to the bound states of the diabatic $B^3\Pi_{0+}$ state.) In the region of $\lambda = 581-590$ nm all resonances except one have very short lifetime and thus only a single vibrational state will contribute significantly to the wave-packet after a few picoseconds. No quantum beats will be seen, which also was found in the experiments. For $\lambda = 564-572$ nm there are two closely spaced states with $\Delta E = 75$ cm^{-1} and $\tau \sim 5-10$ ps. These two states will give rise to quantum beats, as observed in the spectra. The Fourier transform power spectra of the experimental signal gives, however, a spacing of $\Delta E = 48$ cm^{-1}. In the region $\lambda = 551-559$ nm there are several states which are closely spaced and with lifetimes about $\tau = 1-10$ ps. The wave packet will thus consist of several eigenstates for a long time giving rise to a complicated signal. In this region it should be possible to observe revivals of the wave-packet, as is seen in the experiments. The final wave length $\lambda = 547$ nm excites IBr above the dissociation limit, but a few highly excited states might give a small contribution to the signal. In the experiments this is seen as a few initial oscillations and a fast decay. From the Fourier transform power spectra Shapiro *et al.* [17] reports three nearest neighbour differences of 28.7, 31.3 and 33.9 cm^{-1} which they identify with the $\nu = 31-30$, $30-29$ and $29-28$ transitions,

Table 2. Term differences and lifetimes for the IBr $B(^3\Pi_{0+})-Y(0^+)$ interaction. The coupling strength is $V_c = 90$ cm^{-1} and $V_c = 150$ cm^{-1}. The numbering relates to the bound states of the diabatic $B(^3\Pi_{0+})$ state. Figures in parentheses indicates powers of 10.

	Term difference ΔE [cm^{-1}]		Lifetime τ [s]	
ν	90 cm^{-1}	150 cm^{-1}	90 cm^{-1}	150 cm^{-1}
5	111.5	107.9	1.4(−11)	3.0(−12)
6	105.5	100.3	8.6(−13)	2.6(−13)
7	105.4	107.1	1.9(−13)	7.9(−14)
8	115.7	123.9	1.4(−13)	5.3(−14)
9	96.2	120.4	2.4(−10)	5.6(−13)
10	95.1	73.9	2.2(−13)	7.5(−14)
11	83.5	91.5	1.0(−12)	4.1(−12)
12	92.5	102.2	1.9(−12)	3.1(−13)
13	80.6	67.3	3.5(−13)	9.9(−14)
14	72.9	69.9	5.2(−13)	4.3(−13)
15	74.9	82.2	4.1(−12)	4.6(−11)
16	72.5	76.0	1.1(−11)	1.3(−12)
17	67.0	68.5	1.2(−12)	3.0(−13)
18	61.0	56.0	6.3(−13)	1.6(−13)
19	55.9	49.2	5.9(−13)	2.3(−13)
20	52.6	54.1	8.6(−13)	5.7(−13)
21	49.8	52.0	1.7(−12)	1.7(−12)
22	46.4	47.8	4.5(−12)	8.2(−12)
23	42.5	43.4	2.0(−11)	1.7(−09)
24	38.4	39.0	2.6(−09)	1.9(−11)
25	34.3	34.6	5.4(−11)	5.7(−12)
26	30.2	30.3	1.6(−11)	3.2(−12)
27	26.1	26.1	9.6(−12)	2.4(−12)
28	22.1	21.9	7.6(−12)	2.1(−12)
29	18.0	17.8	7.2(−12)	2.0(−12)
30	14.0	13.7	7.9(−12)	2.3(−12)
31	10.0	9.7	1.1(−11)	3.1(−12)
32	6.1	5.7	1.9(−11)	6.1(−12)

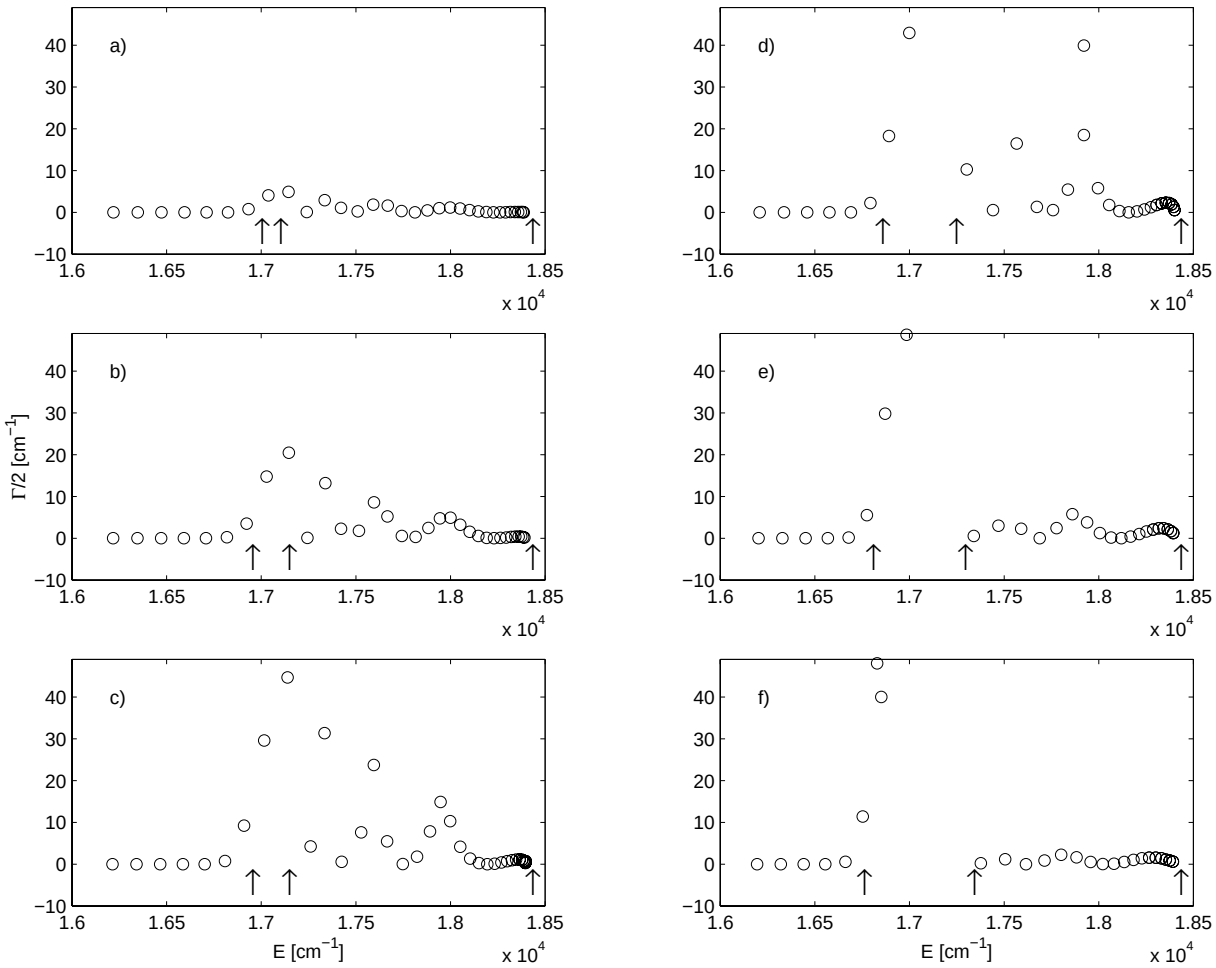

Fig. 3. Predissociation resonances for the IBr $B(^3\Pi_{0+})$–$Y(0^+)$ interaction as a function of coupling strength. (a) $V_c = 50$ cm^{-1}, (b) $V_c = 100$ cm^{-1}, (c) $V_c = 150$ cm^{-1}, (d) $V_c = 200$ cm^{-1}, (e) $V_c = 250$ cm^{-1}, (f) $V_c = 300$ cm^{-1}. Arrows indicate maxima and minima of the adiabatic potential curves near the crossing and the $I(^2P_{3/2}) + Br^*(^2P_{1/2})$ dissociation threshold. Note the oscillatory structure close to the threshold and the emergence of a new dissociation threshold marking a transition from the diabatic to adiabatic picture.

respectively. Our calculations gives 26, 30 and 35 cm^{-1} (with minor differences between $V_c = 90$ and 150 cm^{-1}) which is in reasonable agreement.

In summary the gross features of the experiment can be explained from the resonances computed here but that the details differ, *e.g.* the nearest-neighbour spacings for the highly excited states. For a closer agreement better potential energy surfaces and couplings are needed, the Morse potentials [20] and constant couplings used here can not be used to reproduce the details of the experiments.

5 Summary

To accurately describe a chemical system away from the equilibrium non-adiabatic couplings must be included [1]. This is the rule rather than the exception in photo-chemistry and chemical dynamics. One example is the predissociation caused by a bound state interacting with a dissociative state. In this paper the predissociation resonances of the CO and IBr diatomics have been studied using the DVR-SES method.

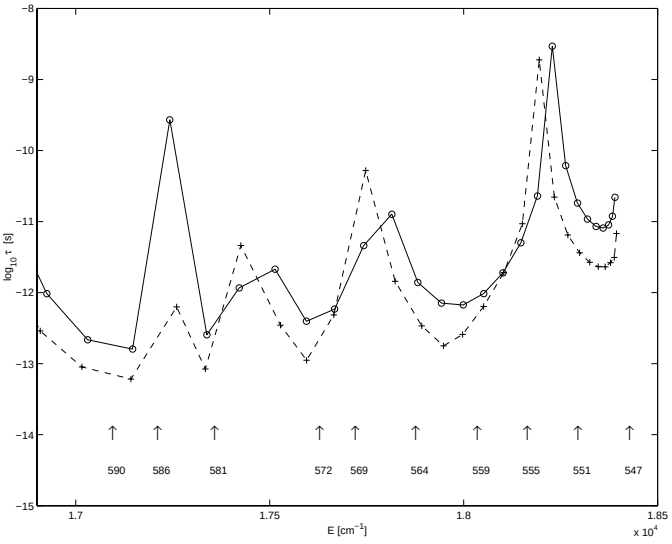

Fig. 4. The resonance lifetimes for $V_c = 90$ cm^{-1} (circles, solid line) and $V_c = 150$ cm^{-1} (pluses, dashed line). Arrows indicate the excitation energies used by Shapiro *et al.* [17].

We first established that the DVR-SES procedure gives as accurate resonances as the DVR-OP and FBR-SES methods for the CO($B^1\Sigma^+ - D'^1\Sigma^+$) predissociation interaction. Then the resonances of the IBr ($B^3\Pi_{0+} - Y0^+$) system was studied. We discussed how the resonance distribution changed with the transition form diabatic (weak coupling) to adiabatic (strong coupling) picture. The main feature of recent pump-probe experiments of the system could be explained but a more detailed description calls for more accurate surfaces and couplings.

The smooth exterior scaling is a robust and effective method. It combines the ease of application from the optical potentials with the rigorous of complex scaling. With no doubt the SES will be of much use in chemical physics for accurate computation of molecular properties involving interactions between bound, continuum and resonances states.

The author would like to thank M. Monnerville and R.J. Buenker for sending their RKR CO surfaces. This work was supported by the Swedish Natural Sciences Research Council (NFR).

References

1. A.J. Alexander, R.N. Zare, J. Chem. Educ. **75**, 1105 (1998).
2. M. Monnerville, J.M. Robbe, J. Chem. Phys. **101**, 7580 (1994).
3. M. Monnerville, J.M. Robbe, Eur. Phys. J. D **5**, 381 (1999).
4. C.C. Marston, G. Balint-Kurti, J. Chem. Phys. **91**, 3571 (1989).
5. D.T. Colbert, W.H. Miller, J. Chem. Phys. **96**, 1982 (1992).
6. B. Fornberg, *A practical guide to pseudospectral methods* (Cambridge University Press, 1996).
7. N. Moiseyev, Phys. Rep. **302**, 211 (1998).
8. Y. Li, O. Bludsky, G. Hirsch, R.J. Buenker, J. Chem. Phys. **107**, 3014 (1997).
9. H.O. Karlsson, J. Chem. Phys. **108**, 3849 (1998).
10. H.O. Karlsson, J. Chem. Phys. **109**, 9366 (1998).
11. N. Moiseyev, J. Phys. B **31**, 1431 (1998).
12. G. Parlant, D.R. Yarkony, IJQC **S26**, 737 (1992).
13. H.O. Karlsson, Phys. Rev. A **50**, 3787 (1994).
14. L.-E. Sedin, Ark. Fys. **29**, 529 (1962).
15. M.S. Child, Mol. Phys. **32**, 1495 (1976).
16. M.J.J. Vrakking, D.M. Villeneuve, A. Stolow, J. Chem. Phys. **105**, 5647 (1996).
17. M. Shapiro, M.J.J. Vrakking, A. Stolow, J. Chem. Phys. **110**, 2465 (1999).
18. M. Shapiro, J. Chem. Phys. **56**, 2582 (1972).
19. A.H. Hussain, G. Roberts, J. Chem. Phys. **110**, 2474 (1999).
20. H. Guo, J. Chem. Phys. **99**, 1685 (1993).